Effect of mix design on the size-independent fracture energy of normal- and high-strength self-compacting concrete

H. Cifuentes✉, J.D. Ríos, E. J. Gómez

ETS Ingeniería, Universidad de Sevilla (Sevilla, Spain)
✉bulte@us.es

ABSTRACT: Self-compacting concrete has a characteristic microstructure inherent to its specific composition. The higher content of fine particles in self-compacting concrete relative to the equivalent vibrated concrete produces a different fracture behavior that affects the main fracture parameters. In this work, a comprehensive experimental investigation of the fracture behavior of self-compacting concrete has been carried out. Twelve different self-compacting concrete mixes with compressive strength ranging from 39 to 124 MPa (wider range than in other studies) have been subjected to three-point bending tests in order to determine the specific fracture energy. The influence of the mix design and its composition (coarse aggregate fraction, the water to binder ratio and the paste to solids ratio) on its fracture behavior has been analyzed. Moreover, further evidence of the objectivity of the size-independent fracture energy results, obtained by the two most commonly used methods, has been provided on the self-compacting concrete mixes.

KEYWORDS: Concrete; Mechanical properties; Microstructure; Mixture proportion; Characterization

RESUMEN: *Influencia de la composición de la mezcla sobre la energía de fractura de hormigones autocompactantes de resistencias media y alta.* Los hormigones autocompactantes tienen una microestructura interna inherente a su composición específica. Su mayor contenido de partículas finas, en comparación con hormigones vibrados equivalentes, provoca un comportamiento diferente en fractura que afecta a los principales parámetros de fractura. En este trabajo, se ha realizado una amplia investigación experimental del comportamiento en fractura de hormigones autocompactantes. Así, se han realizado ensayos de flexión en tres puntos para determinar sus propiedades de fractura sobre 12 hormigones autocompactantes de diferente composición, con resistencias a compresión que van desde 39 hasta 124 MPa (mayor que en otros estudios). De esta forma, se ha analizado la influencia de la dosificación del hormigón y su composición (contenido en árido grueso, relación agua-cemento y pasta-sólidos) sobre su comportamiento en fractura. Además, se ha validado, para hormigones autocompactantes, la objetividad de los resultados obtenidos mediante los dos métodos habitualmente empleados para la determinación de la energía de fractura.

PALABRAS CLAVE: Hormigón; Propiedades mecánicas; Microestructura; Proporción de mezcla; Caracterización

ORCID ID: H. Cifuentes (http://orcid.org/0000-0001-6302-418X); J.D. Ríos (http://orcid.org/0000-0002-2079-5133); E.J. Gómez (http://orcid.org/0000-0002-7770-7640)

1. INTRODUCTION

Self-compacting concrete (SCC) has a different microstructure than the equivalent vibrated concrete (VC) since a higher amount of fine particles in the mix is necessary to comply with the target viscosity and to ensure the necessary flow and passing ability (1,2). This means that the coarse aggregate (CA) content in SCC is usually lower than in the corresponding vibrated concrete and this affects especially its fracture behavior. Cifuentes and Karihaloo (3) performed a comprehensive experimental study to obtain the fracture properties of self-compacting concrete by means of wedge splitting tests (WST) varying the size of the specimens and relative notch depth. They obtained the size-independent fracture energy of concrete by using the boundary effect (BE) method of Hu and Wittmann (4) and verified the applicability of the simplified version (SBE) of the BE method proposed by Abdalla and Karihaloo (5) and validated by Karihaloo et al. (6). They demonstrated that SCC mixes in comparison with equivalent vibrated mixes (with similar compressive strength) show lower values of the size-independent specific fracture energy since the frictional part in the softening branch of the load-displacement or load-CMOD curves is short because of reduced coarse aggregate content. However, the ductility of vibrated concrete mixes is only marginally higher than that of self-compacting concrete mixes due to the influence on other fracture parameters (3). These observations show that a change in the microstructure of the concrete matrix has a significant effect on its fracture properties. Since different mix proportions are possible in order to get similar strength self-compacting concrete mixes (7), a broader study allowing a proper analysis of the influence of the mix design and the various components of the matrix in case of self-compacting concrete is needed.

Nevertheless, the measurement of the fracture properties of concrete in the correct way is crucial to provide reliable results to compare and analyze different concrete mixes. Specifically, the measurement of the specific fracture energy as indicated by RILEM recommendation (8) provides a value that is size-dependent and has to be properly corrected. The most common methods to obtain a size-independent fracture energy of concrete, G_F, are the boundary effect method proposed by Hu and Wittmann (4) or the simplified version (SBE) proposed by Abdalla and Karihaloo (5) and the corrections to the RILEM test proposed by Guinea et al. (9–11). Although the methods are different, they are interrelated since they deal with the treatment of the contribution to the fracture energy when the test is nearing the end and the crack is approaching the back free boundary of the specimen (tail of the P-δ curve). Cifuentes et al. (12) demonstrated that the application of both methods to the same

vibrated concrete mix with a compressive strength of 37 MPa leads to very similar values of G_F. Later on, Murthy et al. (13) provided further experimental evidence of this conclusion using extensive independent test results of three different vibrated concrete mixes ranging in compressive strength from 57 to 122 MPa.

This paper deals with the study of the influence of the components of twelve different self-compacting concrete mixes with compressive strength varying from 39 to 124 MPa on their fracture behavior. In particular, the influence of the coarse aggregate (CA) volume, compressive strength, water to binder (*w/cm*) and paste to solid (*p/s*) ratios on the size-independent fracture energy of concrete (G_F) will be studied using the SBE approach proposed by Abdalla and Karihaloo (5) and the approach proposed by Guinea et al. (9–11). It is shown that the two methods give very similar values of G_F of the SCC mixes. In this manner, very useful information about the influence of the mix proportions, inherent to self-compacting concrete mixes, on their fracture behavior is provided.

2. MATERIALS AND METHODS

The tests described in this paper were conducted on normal and high-strength self-compacting concrete mixes by varying the proportions of the mix (i.e. aggregates volume, paste to solid and water to binder ratios). In this way, SCC mixes with compressive strength ranging from 39 to 124 MPa have been developed. Three-point bending tests were conducted on all mixes to obtain their size-independent specific fracture energy according to the two mentioned methods: the simplified boundary effect method and the approach proposed by Guinea et al. Details of both methods are given in (12).

2.1. Constituents and mix design

In this work, twelve SCC mixes were designed with different volume fractions of coarse aggregate (14), *p/s* and water to binder *w/cm* ratios. The mixes were designed according to the method proposed by Deeb and Karihaloo (15). In every mixture, type II Portland cement produced by Portland Valderrivas cement factory (Seville, Spain) was used to prepare the concrete. A part of the cement was replaced by ground granulated blast furnace slag (ggbs) in normal-strength (NS) SCC or silica fume (SF) in case of high-strength (HS) SCC (16–18). Limestone powder with maximum particle size of 125 *μm* provided by Taljedy factory (Seville, Spain) was used as filler to increase plastic viscosity of the SCC. The fine aggregates (FA) were natural siliceous river sand with a fineness modulus of 2.9 and the coarse aggregates were crushed limestones with the maximum size of 10 mm. Although the nature of

the aggregates affects the fracture behavior of concrete (19,20), this effect is beyond the objective of this study and all mixes were prepared by using the same type of aggregates. A part of the river sand (53%) was replaced by an equivalent volume of the coarser fraction of limestone powder in the size range 125 µm - 2 mm (21). A superplasticizer (SP) of the third generation polycarboxylic ether-based type (Glenium SKY 886) with specific gravity of 1.05 provided by BASF Company was used. The specific gravity of the cement, ggbs and silica fume are 3.10, 3.30 and 2.25, respectively, whereas that of limestone powder, river sand and coarse aggregate are 1.70, 2.65 and 2.8, respectively. These values were measured by using a pycnometer.

The different mixes are divided in two main groups, one group corresponding to NS and the other to HS-SCC. The NS mixes are sub-divided further in three subgroups according to w/cm and p/s ratios. In each group or subgroup the mixes are ordered in descending content of CA. In case of HS mixes, silica fume was employed as cement replacement material in order to obtain a high-strength concrete. The mix proportions and constituents are given in Table 1. After mixing, slump flow tests were conducted on the SCC mixes according to EFNARC guidelines (22) (Table 1).

2.2. Specimen preparation and test procedure

From each of the twelve mixes (Table 1) 10 beam specimens (100 × 100 × 440 mm), four cubes (100 mm) and four cylinders (100 × 200 mm) were

cast. The different types of concrete were produced in a vertical mixer by mixing the coarsest constituent (CA) and the finest one (SF or ggbs), followed by the next coarsest (FA) and next finest constituent (cement), and so on. Before each addition, the constituents were mixed for 2 min. Two-thirds of the super-plasticizer was added to the water in order to fluidize the dry mix. The remaining one-third of the SP was added and mixed for 2 min just before the mix was poured into the moulds. After 24 hours the specimens were demolded and cured in water at ambient temperature for 28 days.

The characteristic compressive strength (f_c) was determined from 100 mm cubes in accordance with UNE EN12930-3:2009. The indirect tensile strength (f_{st}) was obtained using the cylinder splitting test according to UNE EN12930-6:2010, carried out on 100 mm diameter by 200 mm long cylinders. The Young's modulus of concrete (E_c) was determined according to the UNE EN12390-13:2014 by gradually loading a cylindrical specimen in compression to approximately a third of its failure load. The corresponding strain was measured by using two linear transducers (±2.5 mm) aligned with the longitudinal axis of the specimen and mounted between two steel rings, which were concentrically fixed at one third of the height of the specimen respect to its ends. In this way, the reference length to obtain the Young's modulus of the mixes was the central third of the height of the specimens (67 mm).

Regarding the fracture energy of SCC mixes, a three-point bending tests (TPB) were carried out on notched beams according to the RILEM

TABLE 1. Mix proportions (kg/m³) and slump flow test results of SCC mixes

Mix	cm[a] cement	cm[a] ggbs/SF	SP[b]	w/cm	LP[c]	FA[d] FA[†]	FA[d] FA[††]	CA[e]	CA by Vol.	p/s by Vol.	Slump flow Spread (mm)	Slump flow t₅₀₀ (s)
NS-A1	220	135/0	1.8	0.56	61	447	708	556	0.18	0.47	700	2.5
NS-A2	233	118/0	1.8		62	455	790	451	0.15		700	2.5
NS-B1	201	177/0	2.3	0.50	51	377	598	740	0.25	0.47	680	2.8
NS-B2	231	142/0	2.2		54	396	746	581	0.20		695	2.7
NS-B3	245	119/0	2.2		63	459	708	556	0.18		675	2.8
NS-C1	223	174/0	3.4	0.50	51	371	517	786	0.26	0.50	650	2.3
NS-C2	255	131/0	3.3		61	448	531	693	0.23		630	2.3
NS-C3	238	147/0	3.3		59	429	687	543	0.18		660	2.3
NS-C4	296	83/0	3.3		65	477	767	437	0.14		670	2.2
HS-1	431	0/160	17	0.23	54	395	268	958	0.31	0.55	710	2.7
HS-2	421	0/138	17		54	399	564	690	0.23		740	2.8
HS-3	389	0/138	17		54	399	695	564	0.18		750	2.7

[a]cementitious material, i.e. binder (ggbs is the ground granulated blast furnace slag and SF the silica fume).
[b]super-plasticizer (BASF Masterglenium SKY 886).
[c]limestone powder <125 µm.
[d]fine aggregate <2 mm (Note: a part of the fine aggregate is the coarser fraction of the limestone powder, FA[†] 125 µm-2 mm, whereas FA[††] refers to natural river sand <2 mm).
[e]coarse aggregate <10 mm.

work-of-fracture method (8). Four of the beams cast for each mix were notched to a depth of 10 mm (notch to depth ratio $a/W = 0.1$) with a thin (3 mm) diamond saw while the remaining four were notched to a depth of 50 or 60 mm ($a/W = 0.5 – 0.6$). The tests were performed controlling the crack mouth opening displacement (CMOD) by means of a clip gauge transducer. The load-point deflection was measured simultaneously by means of a linearly variable displacement transducer (LVDT) mounted on a rigid frame in order to avoid spurious torsional effects on measurement of vertical displacement. The tests were conducted in a closed-loop dynamic universal testing machine with a maximum load capacity of 50 kN.

3. RESULTS AND DISCUSSION

Table 2 shows the results of the different SCC mixes. Results have been arranged so the mechanical properties (f_c, f_{st} and E_c) are presented first. Then, the fracture properties are shown as obtained by the simplified boundary effect method and the method proposed by Guinea et al. (TA). In case of

SBE method the RILEM size-dependent fracture energy of concrete, G_f, obtained for each SCC mix and relative notch depth are also shown. As main results for this method the transition length, a_l, and the size-independent specific fracture energy, G_F are shown. In case of TA method, the coefficient of adjustment of the tail of the curve A, the displacement δ_u at the end of the test and the size-independent specific fracture energy G_F^* are also presented.

It should be noted in Table 2 that the experimental coefficient of variation (COV) was also calculated for G_F according to the SBE method. This COV is usually not obtained (4,13,23) because of the BE equations must be solved by a least square method for the different RILEM size-dependent fracture energy of concrete, which also have their own associated COV. The SBE is simpler than the BE method since it is not necessary a least square method to solve the system of equations but its basis is the same and the COV associated to this value is not determined. In this work, the COV associated to this experimental method was obtained by considering all

TABLE 2.   Results of mechanical properties and fracture parameters of SCC mixes

Mix	Mechanical properties			Fracture properties (SBE)			Fracture properties (TA)		
	f_c (MPa)	f_{st} (MPa)	E_c (GPa)	α	G_f (N/m)	G_F (N/m)	A (Nmm^2)	δ_u (mm)	G_F^* (N/m)
NS-A1	41 ± 4%	3.5 ± 11%	30.8 ± 14%	0.1	102 ± 1%	122 ± 10%	90 ± 13%	1.09 ± 9%	119 ± 12%
				0.5	85 ± 13%		80 ± 12%	1.43 ± 14%	
NS-A2	40 ± 7%	3.4 ± 5%	30.7 ± 4%	0.1	105 ± 9%	117 ± 13%	80 ± 18%	1.18 ± 16%	114 ± 11%
				0.5	96 ± 17%		118 ± 12%	1.30 ± 18%	
NS-B1	50 ± 3%	4.2 ± 6%	32.1 ± 13%	0.1	141 ± 11%	162 ± 15%	202 ± 13%	1.85 ± 13%	160 ± 8%
				0.5	126 ± 3%		228 ± 15%	1.96 ± 6%	
NS-B2	52 ± 3%	4.0 ± 11%	33.0 ± 5%	0.1	136 ± 10%	149 ± 14%	132 ± 4%	1.47 ± 20%	152 ± 16%
				0.5	127 ± 17%		147 ± 19%	1.59 ± 14%	
NS-B3	51 ± 3%	3.7 ± 5%	30.7 ± 10%	0.1	110 ± 9%	141 ± 18%	119 ± 1%	1.30 ± 18%	134 ± 11%
				0.5	88 ± 16%		89 ± 15%	1.32 ± 4%	
NS-C1	55 ± 2%	3.8 ± 12%	32.4 ± 1%	0.1	132 ± 12%	151 ± 18%	199 ± 14%	2.03 ± 14%	151 ± 12%
				0.6	107 ± 14%		100 ± 20%	2.29 ± 11%	
NS-C2	57 ± 2%	3.9 ± 5%	33.1 ± 1%	0.1	132 ± 7%	145 ± 10%	157 ± 12%	2.06 ± 10%	149 ± 17%
				0.6	116 ± 6%		93 ± 7%	1.62 ± 13%	
NS-C3	53 ± 2%	4.1 ± 6%	30.4 ± 8%	0.1	124 ± 11%	133 ± 14%	61 ± 3%	1.51 ± 16%	136 ± 9%
				0.6	114 ± 9%		69 ± 8%	1.71 ± 17%	
NS-C4	54 ± 3%	4.3 ± 1%	30.3 ± 1%	0.1	103 ± 13%	121 ± 16%	83 ± 19%	1.16 ± 21%	124 ± 15%
				0.6	89 ± 6%		46 ± 17%	1.73 ± 6%	
HS-1	124 ± 3%	6.0 ± 7%	49.1 ± 2%	0.1	139 ± 15%	151 ± 17%	81 ± 19%	1.27 ± 7%	152 ± 12%
				0.6	125 ± 7%		84 ± 18%	1.58 ± 18%	
HS-2	114 ± 3%	5.6 ± 8%	44.2 ± 1%	0.1	118 ± 3%	138 ± 6%	78 ± 11%	1.34 ± 11%	135 ± 11%
				0.6	106 ± 12%		58 ± 23%	1.22 ± 12%	
HS-3	111 ± 4%	5.9 ± 2%	48.9 ± 7%	0.1	115 ± 7%	130 ± 10%	65 ± 14%	1.39 ± 5%	136 ± 6%
				0.6	105 ± 5%		170 ± 16%	1.04 ± 9%	

the possible combinations of the BE equations for the four specimens with the deepest notch depth tested for each mix with the other four specimens corresponding to the shallowest notch depth.

3.1. Mechanical properties

In a recent paper, Abo Dhaheer et al. (2) obtained a formula by a regression analysis of a wide range of data on the compressive strength of SCC that allows to estimate the compressive strength of a SCC mix as a function of its *w/cm* ratio [1]:

$$f_c = \frac{195}{12.65^{w/cm}} \qquad [1]$$

Figure 1 shows the compressive strength as a function of the *w/cm* ratio of the different SCC mixes studied in this work and compares it with the prediction of Eq. [1]. As observed, the prediction given by Eq. [1] fits well, in general, with the obtained experimental results. The deviation with respect to the prediction obtained for some of the mixes is high but it should be taken into consideration that Eq. [1] was obtained by least square fitting of many results obtained from many different researchers and very different SCC mixes (1).

From the results in Table 2, it can be additionally observed that an increase in the paste to solid ratio (*p/s*) leads to a slight increase in the mechanical properties of the SCC mixes, in a similar way to that reported recently by Alyhya et al. (24). A direct comparison of results of the SCC mixes NS-B and NS-C with same *w/cm* ratio but different *p/s* ratios shows that all the mechanical properties of the NS-C mixes (f_c, f_{st} and E_c) with higher *p/s* ratio are slightly higher than those corresponding to NS-B mixes.

The influence of the CA content on the compressive and split tensile strengths obtained for the different mixes of each grade is consistent with that reported by Nikbin et al. (25), namely that they do not follow a definite trend with the coarse aggregate fraction of the mix.
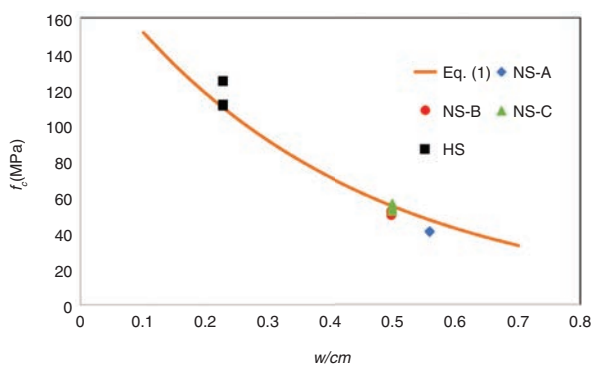
3.2. Influence of the mix composition and strength on fracture energy of SCC

In the following, the analysis of the influence of the coarse aggregate fraction, the water to binder and the paste to solid ratio of the mix composition on fracture energy is made by considering the value of G_F, obtained with the SBE method.

Table 2 shows the variation of G_F with the coarse aggregate fraction for each group of SCC mixes. Direct comparison between mixes of different group is difficult as they have a different range of variation of the coarse aggregate content. However, Figure 2 shows that G_F rises with the increase of the coarse aggregate fraction. This increase is in agreement with previous research on SCC (26) and it is caused by the lengthening of the frictional part of the load-displacement curve (inherent to an increase in the energy dissipation mechanisms: micro-cracking, crack branching, aggregate interlock) and thus, a more pronounced tail of the curve (3).

On the other hand, an increase in the compressive strength should provide an increase in the specific fracture energy since a decrease in the water to binder (*w/cm*) ratio decreases the values of G_F as demonstrated by Beygi et al. (27). Although the range of variation of the coarse aggregate fraction is not the same for the different groups of SCC here analyzed, a comparison of the results of mix NS-A with those of NS-B and NS-C reveals an increase in G_F when the *w/cm* ratio is decreased (Fig. 2). Specifically, if the value of G_F corresponding to NS-A1 mix with a coarse aggregate content of 18% is compared with NS-B3 and NS-C3, with the same CA content but different *w/cm* ratio, it is seen that G_F increases for lower *w/cm* ratios (Fig. 3). As observed, the *p/s* ratio of NS-A1 and NS-B3 is the same and therefore, the trend observed in Figure 3 is not influenced by the *p/s* ratio. It should be noted that although the HS-B3 mix has the same CA content, was not used in this comparative analysis since its fracture energy does not follow the same trend with the *w/cm* ratio because of the

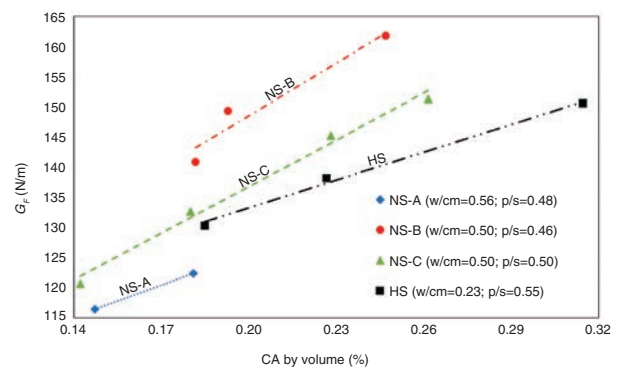FIGURE 1. Relation between compressive strength and *w/cm* ratio.

FIGURE 2. Variation of G_F with the volume fraction of coarse aggregate.

presence of silica fume instead of ggbs. The use of silica fume produces a densification in the interfacial transition zone (ITZ), which implies a decrease of G_F (3).

Regarding the p/s ratio of the SCC mixes, its influence on the specific fracture energy of concrete is evidenced in different ways. On the one hand, direct comparison of values obtained for NS-B and NS-C mixes with same w/cm ratio but different p/s ratio shows a decrease in G_F with an increase in the p/s. This effect was also observed by Alyhya et al. (24), as they obtained a noticeable decrease in G_F with an increase in the p/s ratio for different SCC mixes with compressive strength ranging from 30 to 80 MPa. Nevertheless, if the values obtained for the HS mixes are compared with the analogous values for NS mixes it is observed that there is no increase in the values of G_F with a decrease in the w/cm ratio, as might have been expected. This is due to the fact that the decrease in G_F produced by an increase in the p/s ratio outstrips the increase produced in it by a decrease in w/cm. Moreover, in case of HS mixes silica fume was employed instead of ggbs. As mentioned before, the use of silica fume in SCC produces a densification in the ITZ that leads to a stiffer cementitious matrix (28) so that the frictional part of the P-δ curve is shorter in comparison with normal-strength SCC mixes. This effect was previously observed by Cifuentes and Karihaloo (3) who found that fracture energy decreased from 151.8 N/m for a w/cm ratio of 0.48 (normal strength SCC with $f_c = 41.0$ MPa) to 88.7 N/m for a w/cm ratio of 0.23 (high-strength SCC with $f_c = 97.7$ MPa).
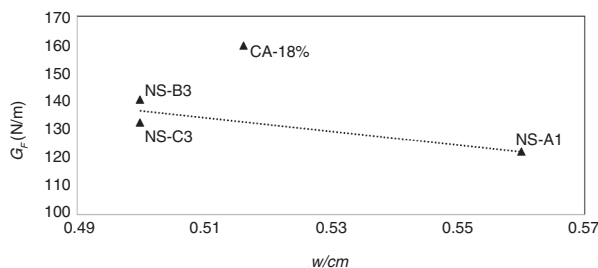

FIGURE 3. Variation of G_F with w/cm ratio for NS-A1, NS-B3 and NS-C3.
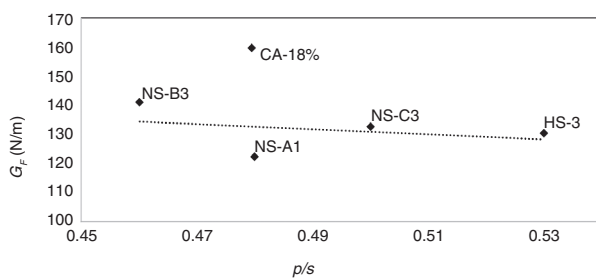

FIGURE 4. Variation of G_F with p/s ratio for NS-A1, NS-B3, NS-C3 and HS-3 mixes with the same CA content.

They concluded that this decrease in G_F was due to the densification of the matrix produced by the use of a higher content of fine particles, especially silica fume, in high-strength SCC mixes. In Fig. 4, the variation of G_F with the p/s ratio for NS-A1, NS-B4, NS-C3 and HS-3 with the same CA content (18%) is represented, where the decrease in G_F with increasing p/s ratio is observed.

Although the trend of the mean values of G_F shown in Figures 4 and 5 is similar to that obtained by other researchers, it should be noted that the experimental confirmation of these phenomena is weaker in this case because of the high values of the COV and the small range of variation of the w/cm and p/s ratios between SCC mixes. However, the finding of a reasonable trend of the variation of G_F with the constituents of the mixes is an evidence of the reliability of results.

3.3. Influence of the method employed for determining the size-independent fracture energy

Table 2 compares the mean values of the size-independent specific fracture energy of all concrete mixes obtained by using the two methods described above (G_F for SBE method and G_F^* for the TA method). It is evident that both methods give very similar values of the mean size-independent specific fracture energies. This conclusion was previously reported by Cifuentes et al. (12) and by Murthy et al. (13) for different strengths of vibrated concrete (VC). Although these two methods use very different experimental procedures, they are closely interrelated as both procedures apply some corrections to the final part of the P–δ curve in the RILEM work-of-fracture test (29). The BE method considers the influence on G_F when the crack approaches the back free boundary of the specimen in the final part of the test (4), whereas the method of Guinea et al. (11) is mainly based on the determination of the non-measured work-of-fracture by adjusting the tail of the load-displacement curve that also corresponds to the end of the test.

The results confirm the similarity of the size-independent fracture energy obtained by either of the methods (SBE or TA) for self-compacting concrete with compressive strength ranging from the lowest value of 39.8 MPa corresponding to mix NS-A2 to the highest value of 124.0 MPa of HS-1.

3.4. Bilinear tension softening diagram

Another important fracture property of a concrete mix is the bilinear tension softening diagram, which becomes an essential parameter when a numerical analysis of the fracture behavior of concrete is necessary. The parameters of the diagram corresponding to the size-independent specific fracture energy for each SCC mixes are determined by

an inverse analysis according to the non-linear hinge model described in (30,31). Since an analysis of the influence of the microstructure of SCC mixes is performed in this work, it should be pointed out that the bilinear tension softening diagram (Figure 5) captures the micro-cracking and frictional dissipation processes responsible for the observed post-peak behavior in a concrete mix (24). The first steep linear branch of the softening diagram is due to the micro-cracking, whereas the shallow second linear branch is a consequence of the frictional dissipation processes, e.g. aggregate interlock.

The determination of the bilinear softening diagrams consists of the minimization of the sum of the square errors between the experimental and theoretical values of the load obtained for each CMOD value according to the analytical expressions given in (31). Results of the theoretical load-CMOD curves for some SCC mixes and relative notch depths are shown in Figure 6.

As two different relative notch depths were tested according to the SBE method, the parameters
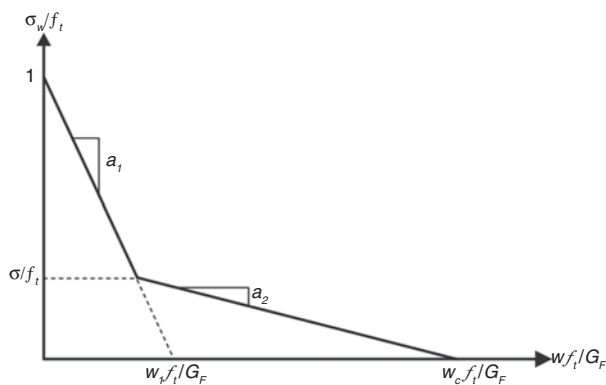

FIGURE 5. Bilinear softening diagram.

defining the bilinear softening diagram of each mix need to be properly scaled to avoid the size dependency of its specific fracture energy. The bilinear softening diagrams of all twelve SCC mixes corresponding to G_F are shown in Figure 7. The values of the three parameters defining the softening diagrams are shown in Table 3.

The obtained values of a_1, which corresponds to the slope of the first steep branch of the bilinear softening diagram (Figure 5), increases with an increase of the coarse aggregate volume fraction and the paste to solid ratio, as previously observed by Alyhya et al. (24). Analogously, the critical opening displacement (w_c) is influenced by the CA and the w/cm ratio, increasing with an increase of CA and a decrease of w/cm ratio. The influence of the p/s ratio is specially felt in case of high-strength mixes where silica fume was employed and a more densified matrix is obtained. For these HS mixes the increase of the p/s ratio outstrips again the decrease of the w/cm ratio as their values of w_c are lower than the analogous values for NS mixes.

Another important aspect of the softening diagram is the estimation of the direct tensile strength (f_t) of the SCC mixes. Table 5 shows the relationship between the direct and splitting tensile strengths (f_t/f_{st}) obtained for all mixes. In most cases, the values are lower than the usual value of 2/3 for VC (32). As observed, this relationship is specially influenced by p/s and the w/cm ratios of the mix, increasing with an increase in p/s and a decrease in w/cm ratio as previously demonstrated by Alyhya et al. (24).

3.5. Ductility

A detailed analysis of the fracture behavior of the self-compacting concrete mixes can be made through the ductility of concrete. This ductility is
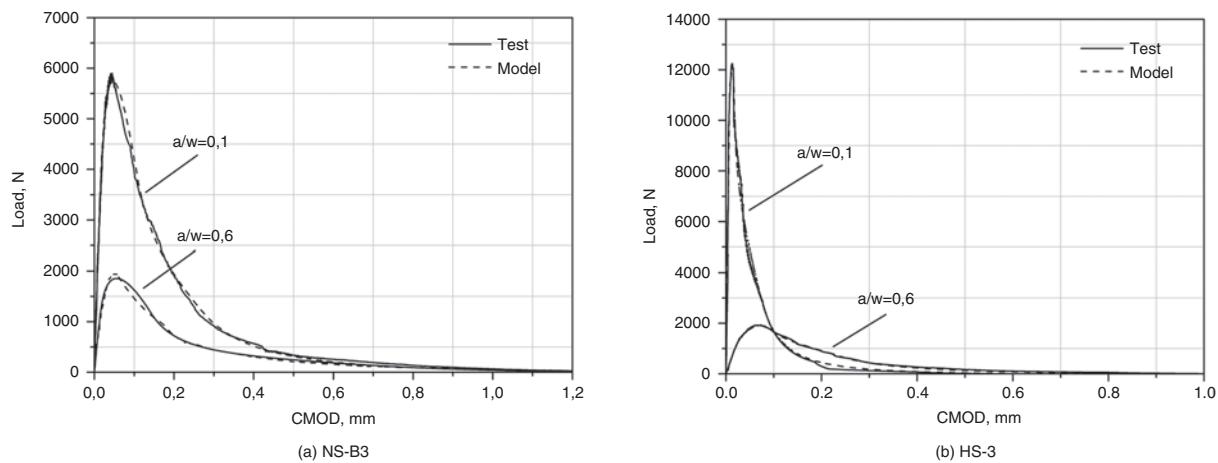

(a) NS-B3

(b) HS-3

FIGURE 6. Representative Load-CMOD curves generated by the hinge model and average experimental load-CMOD curves for NS- (a) and HS-SCC mixes (b).
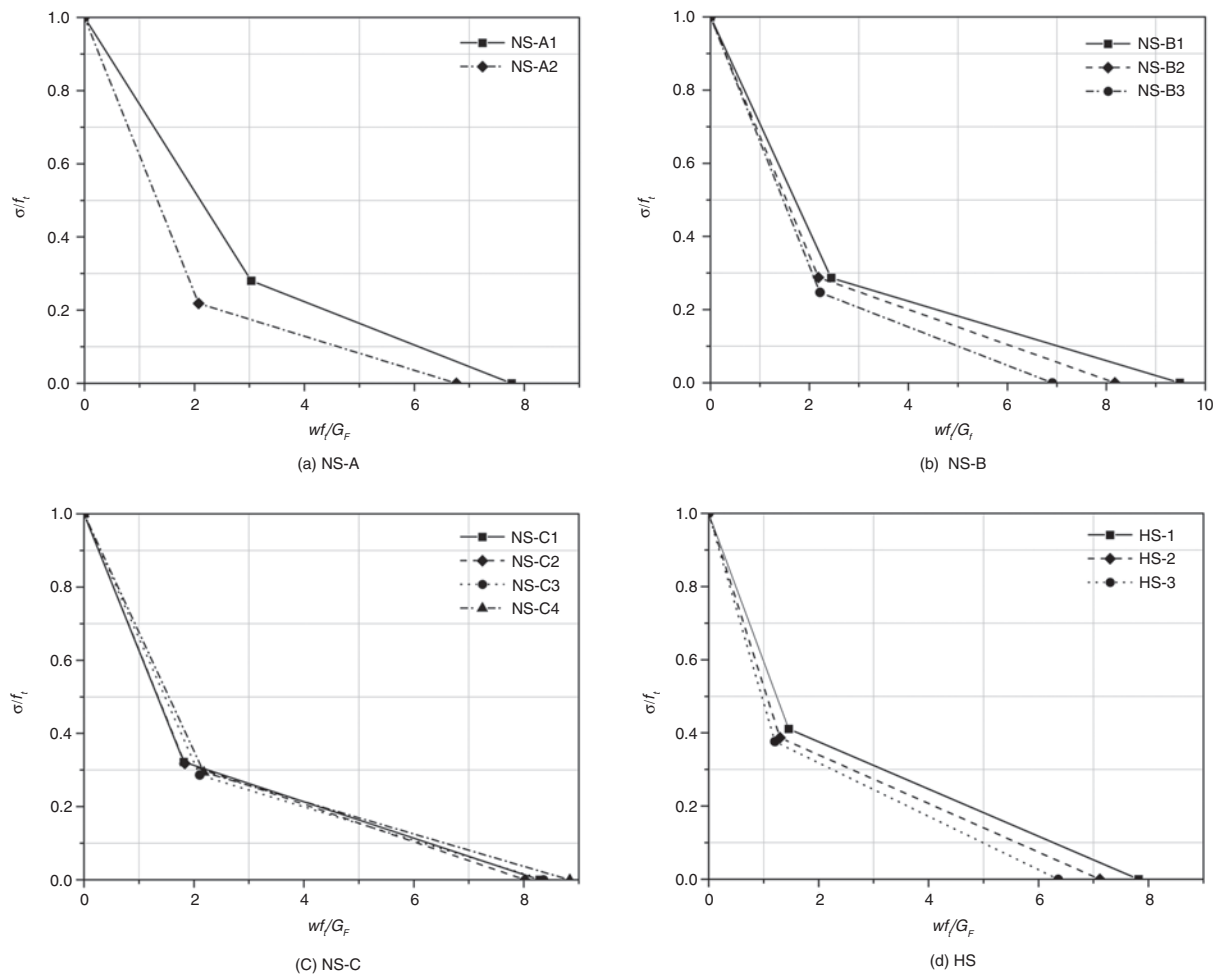
FIGURE 7. The normalised bilinear stress-crack opening relationship for different SCC grades corresponding to their size-independent fracture energy (G_F).

quantified by means of the characteristic length, l_{ch} given by the following expression [2]:

$$l_{ch} = \frac{E_c G_F}{f_{st}^2} \qquad [2]$$

The characteristic length was proposed by Hillerborg et al. (33) and is an important fracture parameter related with the ductile/brittle behavior of the concrete mix.

The analysis of the ductility provides interesting information about the fracture behavior of SCC as the characteristic length relates properties of concrete on which the specific composition of self-compacting concrete has different effects. Due to the denser interfacial transition zone (ITZ) of SCC compared with a similar strength VC (27) the G_F of SCC is usually lower than the value corresponding to an equivalent VC, which contains a higher fraction of the coarse aggregate. However, in SCC the internal stiffness of the matrix of the mix is usually higher and the tensile strength lower than in

equivalent VC because it contains a higher content of fine particles (3). Consequently, the composition and strength of the mix play an important role in the ductile/brittle behavior of SCC (24).

Table 3 also shows the l_{ch} values obtained for all the mixes corresponding to each grade. As observed, the characteristic length changes between 340 and 182 mm for compressive strength range between 40 and 124 MPa.

In Figure 8 l_{ch} is plotted for the different SCC mixes. As it can be seen in Fig. 8 the most important parameter affecting l_{ch} is the tensile strength since the ductility of concrete decreases as w/cm ratio decreases, causing SCC to have less ductile (or more brittle) behavior. This effect was confirmed by other authors (27) and it can be attributed to the change in concrete fractal dimension (34) due to a higher rupture in aggregate phase for high-strength SCC mixes.

Since the mixes for each type of concrete are designated in order of decreasing fraction of coarse aggregate, it can be observed that the values of l_{ch}

TABLE 3.   Parameters of the bilinear softening diagram corresponding to the size-independent specific fracture energy (G_F)

Mix Designation	a_1	a_2	w_1 mm	w_c mm	$\dfrac{\sigma}{f_t}$	f_t MPa	f_t / f_{st}	Mean f_t / f_{st}
NS-A1	0.237 ± 8%	0.059 ± 3%	0.143 ± 3%	0.263 ± 9%	0.280	2.10 ± 10%	0.61	0.63
NS-A2	0.377 ± 9%	0.037 ± 10%	0.089 ± 2%	0.266 ± 2%	0.218	2.14 ± 10%	0.64	
NS-B1	0.292 ± 7%	0.041 ± 4%	0.130 ± 9%	0.360 ± 5%	0.287	2.40 ± 8%	0.57	0.64
NS-B2	0.327 ± 4%	0.048 ± 10%	0.116 ± 7%	0.310 ± 5%	0.288	2.44 ± 8%	0.61	
NS-B4	0.341 ± 5%	0.053 ± 12%	0.106 ± 8%	0.250 ± 3%	0.247	2.35 ± 9%	0.64	
NS-C1	0.374 ± 10%	0.050 ± 4%	0.106 ± 9%	0.330 ± 5%	0.322	2.61 ± 2%	0.69	0.66
NS-C2	0.372 ± 4%	0.051 ± 3%	0.106 ± 3%	0.307 ± 7%	0.318	2.70 ± 8%	0.69	
NS-C3	0.339 ± 10%	0.046 ± 5%	0.098 ± 4%	0.278 ± 8%	0.286	2.55 ± 7%	0.62	
NS-C4	0.324 ± 7%	0.044 ± 2%	0.089 ± 7%	0.255 ± 10%	0.294	2.67 ± 5%	0.63	
HS-1	0.404 ± 10%	0.065 ± 1%	0.063 ± 10%	0.198 ± 9%	0.411	3.81 ± 8%	0.64	0.69
HS-2	0.472 ± 9%	0.067 ± 5%	0.051 ± 3%	0.172 ± 2%	0.387	3.78 ± 8%	0.68	
HS-3	0.519 ± 9%	0.073 ± 10%	0.044 ± 3%	0.146 ± 4%	0.376	3.90 ± 4%	0.66	
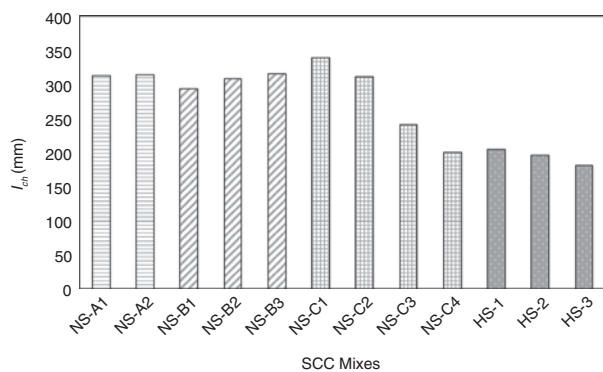
FIGURE 8.   Variation of l_{ch} for the different SCC mixes.

does not follow a clear trend because of the influence of the tensile strength. Only in case of NS-C and HS mixes, l_{ch} tend to decrease when the CA fraction decreases due to the strong effect of the CA obtained for these mixes. The increase of G_F with the increase of the coarse aggregate fraction is clear as demonstrated in this study and previous work from other authors (27). As regards the tensile strength of SCC for each grade there is no definite trend with the CA fraction (25), which produces a fluctuation of the values of l_{ch} with CA for each grade due to its great influence in Eq. (2). As observed in Figure 8 the increase of the tensile strength produces a decrease of l_{ch} due to the reduction of w/cm ratio. However, the change is not as abrupt as it can be expected according to the compressive strength change of the mix from normal-strength to high-strength SCC mixes. This effect is due to the utilization of silica fume as cementitious material in high-strength SCC mixes and the subsequently densification of the ITZ (26). Although G_F slightly decrease with the utilization of silica fume as demonstrated before, the internal stiffness of the matrix of the SCC mixes is higher and the increase of tensile strength is not so pronounced because they contain a higher content of cementitious materials and are more susceptible to cracking (3).

4. CONCLUSIONS

From the extensive investigation reported above, the following conclusions can be drawn:

- The results show that the size-independent fracture energy of self-compacting concrete can be obtained by means of two methods (SBE and the method proposed by Guinea et al.). The results are very similar and they are independent of the employed method. Although other authors have postulated this conclusion, it has been demonstrated to be so for SCC mixes with a wide compressive strength range.
- An increase in the coarse aggregate fraction produces an increase in the size-independent fracture energy. This conclusion has been extended for a wider range of compressive strength of the SCC mixes than reported by other authors.
- A decrease in w/cm produces an increase in G_F.
- The p/s ratio of the mix has influence on G_F. Mixes with higher p/s ratio shows a lower value of the size-independent fracture energy.
- The use of silica fume in high-strength SCC mixes produces a densification in the interfacial transition zone, which leads to a lower value of G_F.
- The ratio between the direct tensile strength and the split tensile strength of the SCC mixes increases with the reduction of the CA content and the w/cm and p/s ratios.
- The coarse aggregate fraction increases the ductility of concrete, as quantified by means of l_{ch}.

- A decrease in the *w/cm* ratio decreases the ductility of concrete as the compressive strength of concrete increases. In case of high-strength SCC mixes, the use of silica fume produces the densification of the ITZ and subsequently increases the Young modulus of concrete more sharply than its tensile strength.

ACKNOWLEDGEMENTS

REFERENCES

1. Abo Dhaheer, M.S.; Al-Rubaye; M.M.; Alyhya, W.S.; Karihaloo, B.L.; Kulasegaram, S. (2015) Proportioning of self–compacting concrete mixes based on target plastic viscosity and compressive strength: mix design procedure. *J. Sustain. Cem. Mater.* 5[4], 199–216. https://doi.org/10.1080/21650373.2015.1039625

2. Abo Dhaheer, M.S.; Al-Rubaye; M.M.; Alyhya, W.S.; Karihaloo, B.L.; Kulasegaram, S. (2015) Proportioning of self-compacting concrete mixes based on target plastic viscosity and compressive strength: experimental validation. *J. Sustain. Cem. Mater.* 5[4], 217–232. https://doi.org/10.1080/21650373.2015.1036952

3. Cifuentes, H.; Karihaloo, B.L. (2013) Determination of size-independent specific fracture energy of normal- and high-strength self-compacting concrete from wedge splitting tests. *Constr. Build. Mater.* 48, 548–553. https://doi.org/10.1016/j.conbuildmat.2013.07.062

4. Hu, X.Z.; Wittmann, F.H. (1992) Fracture energy and fracture process zone. *Mater. Struct.* 25[6], 319–326. https://doi.org/10.1007/BF02472918

5. Abdalla, H.M.; Karihaloo, B.L. (2003) Determination of size-independent specific fracture energy of concrete from three-point bend and wedge splitting tests. *Mag. Concr. Res.* 55[2], 133–141. https://doi.org/10.1680/macr.2003.55.2.133

6. Karihaloo, B.L.; Abdalla, H.M.; Imjai, T. (2003) A simple method for determining the true specific fracture energy of concrete. *Mag. Concr. Res.* 55[5], 471–481. https://doi.org/10.1680/macr.55.5.471.37590

7. Karihaloo, B.L.; Ghanbari, A. (2012) Mix proportioning of self-compacting high- and ultra-high-performance concretes with and without steel fibres. *Mag. Concr. Res.* 64[12], 1089–1100. https://doi.org/10.1680/macr.11.00190

8. RILEM (1985) Determination of the fracture energy of mortar and concrete by means of three-point bend tests on notched beams. *Mater. Struct.* 18[4], 287–290. https://doi.org/10.1007/BF02472918

9. Guinea, G.V.; Planas, J.; Elices, M. (1992) Measurement of the fracture energy using three-point bend tests: Part 1-Influence of experimental procedures. *Mater. Struct.* 25[4], 212–218. https://doi.org/10.1007/BF02473065

10. Planas, J.; Elices, M.; Guinea, G.V. (1992) Measurement of the fracture energy using three-point bend tests: Part 2-Influence of bulk energy dissipation. *Mater. Struct.* 25[5], 305–312. https://doi.org/10.1007/BF02472671

11. Elices, M.; Guinea, G.V.; Planas, J. (1992) Measurement of the fracture energy using three-point bend tests: Part 3-Influence of cutting the P-d tail. *Mater. Struct.* 25[6], 327–334. https://doi.org/10.1007/BF02472591

12. Cifuentes, H.; Alcalde, M.; Medina, F. (2013) Measuring the size-independent fracture energy of concrete. *Strain* 49[1], 54–59. https://doi.org/10.1111/str.12012

13. Murthy, A.R.; Karihaloo, B.L.; Iyer, N.R.; Raghu Prasad, B.K. (2013) Determination of size-independent specific fracture energy of concrete mixes by two methods. *Cem. Concr. Res.* 50, 19–25. https://doi.org/10.1016/j.cemconres.2013.03.015

14. Pavía, S.; Aly, M. (2016) Influence of aggregate and supplementary cementitious materials on the properties of hydrated lime (CL90s) mortars. *Mater. Construcc.* 66[324], e104. https://doi.org/10.3989/mc.2016.01716

15. Deeb, R.; Karihaloo, B.L. (2013) Mix proportioning of self-compacting normal and high-strength concretes. *Mag. Concr. Res.* 65[9], 546–556. https://doi.org/10.1680/macr.12.00164.

16. Bonavetti, V.L.; Castellano, C.; Donza, H.; Rahhal, V.F.; Irassar, E.F. (2014) Cement with silica fume and granulated blast-furnace slag: strength behavior and hydration. *Mater. Construcc.* 64 [315], e025. https://doi.org/10.3989/mc.2014.04813

17. Rozas, F.; Castillo, A.; Martínez, I.; Castellote, M. (2015) Guidelines for assessing the valorization of a waste into cementitious material: dredged sediment for production of self compacting concrete. *Mater. Construcc.* 65 [319], e057. https://doi.org/10.3989/mc.2015.10613

18. Ince, C.; Derogar, S.; Michelitsch, T.M. (2015) Influence of supplementary cementitious materials on water transport kinetics and mechanical properties of hydrated lime and cement mortars. *Mater. Construcc.* 65 [318], e056. https://doi.org/10.3989/mc.2015.05214

19. Ruiz, G.; Zhang, X.X.; Yu, R.C.; Porras, R.; Poveda, E.; Del Viso, J.R. (2011) Effect of loading rate on fracture energy of high-strength concrete. *Strain* 47[6], 518–524. https://doi.org/10.1111/j.1475-1305.2010.00719.x

20. Zhang, X.; Ruiz, G.; Yu, R.C.; Poveda, E.; Porras, R. (2012) Rate effect on the mechanical properties of eight types of high-strength concrete and comparison with FIB MC2010. *Constr. Build. Mater.* 30, 301–308. https://doi.org/10.1016/j.conbuildmat.2011.11.037

21. Fernández-Ledesma, E.; Jiménez, J.R.; Ayuso, J.; Corinaldesi, V.; Iglesias-Godino, F.J. (2016) A proposal for the maximum use of recycled concrete sand in masonry mortar design. *Mater. Construcc.* 66 [321], e075. https://doi.org/10.3989/mc.2016.08414

22. EFNARC (2005) The European guidelines for self-compacting concrete-specification, production and use. http://www.efnarc.org

23. Muralidhara, S.; Raghu Prasad, B.K.; Karihaloo, B.L.; Singh, R.K. (2011) Size-independent fracture energy in plain concrete beams using tri-linear model. *Constr. Build. Mater.* 25[7], 3051–3058. https://doi.org/10.1016/j.conbuildmat.2011.01.003

24. Alyhya, W.S.; Abo Dhaheer, M.S.; Al-Rubaye, M.M.; Karihaloo, B.L. (2016) Influence of mix composition and strength on the fracture properties of self-compacting concrete. *Constr. Build. Mater.* 110, 312–322. https://doi.org/10.1016/j.conbuildmat.2016.02.037

25. Nikbin, I.M.; Beygi, M.H.A.; Kazemi, M.T.; Vaseghi Amiri, J.; Rahmania, E.; Rabbanifara, S.; Eslamic, M. (2014) A comprehensive investigation into the effect of aging and coarse aggregate size and volume on mechanical properties of self-compacting concrete. *Mater. Des.* 59, 199–210. https://doi.org/10.1016/j.matdes.2014.02.054

26. Beygi, M.H.A.; Kazemi, M.T.; Nikbin, I.M.; Vaseghi Amiri, J.; Rabbanifara, S.; Rahmania, E. (2014) The influence of coarse aggregate size and volume on the fracture behavior and brittleness of self-compacting concrete. *Cem. Concr. Res.* 66, 75–90. https://doi.org/10.1016/j.cemconres.2014.06.008

27. Beygi, M.H.A.; Kazemi, M.T.; Nikbin, I.M.; Vaseghi Amiri, J. (2013) The effect of water to cement ratio on fracture parameters and brittleness of self-compacting concrete. *Mater. Des.* 50, 267–276. https://doi.org/10.1016/j.matdes.2013.02.018

28. Akçaoğlu, T.; Tokyay, M.; Çelik, T. (2004) Effect of coarse aggregate size and matrix quality on ITZ and failure behavior of concrete under uniaxial compression. *Cem. Concr. Compos.* 26[6], 633–638. https://doi.org/10.1016/S0958-9465(03)00092-1

29. Vydra, V.; Trtík, K.; Vodák, F. (2012) Size independent fracture energy of concrete. *Constr. Build. Mater.* 26[1], 357–361. https://doi.org/10.1016/j.conbuildmat.2011.06.034
30. Murthy, A.R.; Karihaloo, B.L.; Iyer, N.R.; Raghu Prasad, B.K. (2013) Bilinear tension softening diagrams of concrete mixes corresponding to their size-independent specific fracture energy. *Constr. Build. Mater.* 47, 1160–1166. https://doi.org/10.1016/j.conbuildmat.2013.06.004
31. Abdalla, H.M.; Karihaloo, B.L. (2004) A method for constructing the bilinear tension softening diagram of concrete corresponding to its true fracture energy. *Mag. Concr. Res.* 56[10], 597–604. https://doi.org/10.1680/macr.2004.56.10.597

32. Neville, A.M. (1995) Properties of Concrete, 4th ed. Longman. London.
33. Hillerborg, A.; Modéer, M.; Petersson, P.E. (1976) Analysis of crack formation and crack growth in concrete by means of fracture mechanics and finite elements. *Cem. Concr. Res.* 6[6], 773–781. https://doi.org/10.1016/0008-8846(76)90007-7
34. Yan, A.; Wu, K.R.; Zhang, D.; Yao, W. (2001) Effect of fracture path on the fracture energy of high-strength concrete. *Cem. Concr. Res.* 31[11], 1601–1606. https://doi.org/10.1016/S0008-8846(01)00610-X